A base-level stratigraphic approach to determining Holocene subsidence of the Ganges–Meghna–Brahmaputra Delta plain

Céline Grall, M.S. S Steckler, J.L. L Pickering, S. Goodbred, R. Sincavage, C. Paola, S.H. Akhter, V. Spiess

Earth and Planetary Science Letters 499 (2018) 23–36

Contents lists available at ScienceDirect

Earth and Planetary Science Letters

www.elsevier.com/locate/epsl

A base-level stratigraphic approach to determining Holocene subsidence of the Ganges–Meghna–Brahmaputra Delta plain

C. Grall [a,*], M.S. Steckler [a], J.L. Pickering [b], S. Goodbred [b], R. Sincavage [c], C. Paola [d], S.H. Akhter [e], V. Spiess [f]

[a] Lamont-Doherty Earth Observatory of Columbia University, NY, USA
[b] Vanderbilt University, TN, USA
[c] Radford University, Radford, VA, USA
[d] University of Minnesota-Twin Cities, Minneapolis, MN, USA
[e] Dhaka University, Dhaka, Bangladesh
[f] University of Bremen, Bremen, Germany

ARTICLE INFO

Article history:
Received 7 August 2017
Received in revised form 7 May 2018
Accepted 7 July 2018
Available online 26 July 2018
Editor: A. Yin

Keywords:
Ganges–Brahmaputra–Meghna Delta
subsidence
relative sea level
delta plain
base level stratigraphic method
indicative meaning of sea level index

ABSTRACT

Relative sea level history, which is the result of the combined effects of land subsidence, sediment supply and absolute sea level history may be reconstructed from preserved sediment thicknesses. However, variations in the preserved sediment thicknesses between different sedimentary environments strongly limit the accuracy of this type of geological approach, particularly in fluvial channelized systems, such as delta plains. To address this, we apply three different and independent stratigraphic approaches to the case of the Ganges–Brahmaputra–Meghna Delta (GBMD). Our approach has been made possible by a broad dataset of geological archives we have collected, which includes more than 400 hand-drilled stratigraphic wells, 198 radiocarbon ages, and river seismic reflection data (255 km of high-resolution multichannel seismic images). The seaward gradient of accommodation and the limit of the subsiding delta plain are estimated, assuming that the delta is near or at the base-level, which is considered to be the relative sea-level. First, a statistical analysis of the variability of preserved sediment thicknesses is used to derive the average pattern of accommodation from the Holocene isopach. Secondly, the preserved sediment thicknesses are analyzed by geomorphotectonic domains to estimate an average pattern of accommodation. Thirdly, the burial history of the seismically imaged last glacial incision of the Brahmaputra River is reconstructed. Results suggest that the variability of preserved sediment thicknesses can be up to 35% in a delta plain between river channel and flood plain deposits for the same relative sea-level history. Taking this variability into consideration, the Holocene relative sea-level history of the GBMD and the most likely pattern of subsidence are determined. Results provide evidence of moderate Holocene subsidence over the delta, gently increasing seaward from <0.2 mm/yr landward of the Hinge Zone, which can be considered as the northern limit of the subsiding delta plain, to 2 ± 0.7 mm/yr in the middle fluvial delta to 4 ± 1.4 mm/yr in the lower tidal delta. This enables us to construct the first millennial-scale map of subsidence pattern on the GBMD in which uncertainties on subsidence rates are provided. This map may aid in evaluating the negative impact that human modification may have on subsidence and relative sea level in the GBMD, and thereby help to determine better sustainable coastal management practices for the GBMD and other large delta plains.

1. Introduction

Deltas are important environments that are home to hundreds of millions of people and multiple megacities. They are highly productive for both agriculture and aquaculture, as well as extractive industries, such as oil and gas. They are also highly vulnerable to increasing rates of sea-level rise and the associated natural hazards (Syvitski et al., 2009; Schmidt, 2015; Ericson et al., 2006; Foufoula-Georgiou, 2013; Giosan et al., 2014; Anthony et al., 2015). Indeed, these low-lying environments at the boundary between land and ocean represent a fragile balance between changing sea level, land subsidence, and sediment supply. Geological archives are a precious source for providing information about this fragile balance, as the relative sea-level history, which represents the interplay of these three parameters (Miall and Miall, 2001) can be recon-

* Corresponding author.
E-mail address: cgrall@ldeo.columbia.edu (C. Grall).

https://doi.org/10.1016/j.epsl.2018.07.008

structed from them. These geological archives can provide sea-level index points (aka SLIPs, Shennan, 2007) that may be stratigraphically determined from the records of sediment accumulation. However, assessing the natural variability of sedimentary systems and the pattern of subsidence in the geological archives is a persistent challenge. Indeed, variability within depositional systems can create noise in the data that can be misinterpreted as differences in subsidence rate. For example, lateral river channel shifts can produce both erosion and rapid accumulation of sediments. Rapidly filled in abandoned channels can be misinterpreted as rapid subsidence. In addition, the continuing subsurface evolution of geological archives during their burial histories add to the complexity of stratigraphic reconstructions. For instance, oxidation of organic matter, such as peats, and shallow compaction can produce large local apparent subsidence rates in the short term. All those factors result in a confusing pattern of subsidence over delta plains. This is particularly true in the highly dynamic Ganges–Brahmaputra Meghna Delta (GBMD) (e.g., Brown and Nicholls, 2015).

The GBMD is the largest and most densely populated delta in the world, covering ~100,000 km^2 with a population of over 130,000,000 people. The GBMD is susceptible to riverine flooding, flash flooding and tropical cyclones (Chiu and Small, 2016; Chaumillon et al., 2017), which places the region at high risk for storm disasters and flooding (Siddique and Euosof, 1987; Bern et al., 1993; Paul, 2009; Mallick et al., 2011). These hazards may be amplified by rapid land subsidence (Chaumillon et al., 2017). The GBMD is placed among the most at risk deltas by Tessler at al. (2015) and Ericson et al. (2006). However, the rate of subsidence of the GBMD is highly uncertain and spatially variable. Most of the rates provided in the literature are summarized in the review paper by Brown and Nicholls (2015), which compiled an extensive list of the limited, but variable, available measurements. This review includes subsidence estimates from tide gauges (Syvitski et al., 2009), from geological records (Alam et al., 2003; Hoque and Alam, 1997; Umitsu, 1993; Stanley and Hait, 2000 and Goodbred and Kuehl, 2000a), from historical records (Sarker et al., 2012; Hanebuth et al., 2013) and from InSAR data (Higgins et al., 2014). The mixing of multiple methods and time scales, though, results in a wide range of reported subsidence values from −1 to 44 mm/yr, with considerable scatter even at individual sites. In all, the ensemble of published rates presents a confusing picture of subsidence patterns for the GBMD, yet a better understanding is essential to assessing the risks facing this densely populated region in response to increasing rates of sea-level rise and associated natural hazards. While some of the observed variability is certainly real, there is a considerable amount of scatter that comes from neglecting the variability in depositional systems and burial histories of geological archives.

In order to determine the pattern of subsidence over the GBMD, we analyze the stratigraphic records over the Holocene by using three independent methods and develop a new and simple analytical stratigraphic method to take into account the variability in sediment infilling rates that are associated with channel incision from the shifting rivers. Our approach has been made possible by a large dataset that includes sediment accumulation measurements from >400 tube wells with age constraints from 198 ^{14}C ages, and a high resolution multichannel seismic line on the Jamuna (Brahmaputra) River. Our results provide a new, more coherent picture of the subsidence pattern and rates due to natural processes on the GBMD for the Holocene. This improved subsidence map may, in turn, help to better understand the significant impacts that human activities are currently having on the delta and the extent of impacts that may occur in the future.

2. Geological setting

2.1. Stratigraphic context of the GBMD during the Holocene

During the Holocene, eustatic sea level rose ~60 m in two phases. During the early to the mid Holocene (Walker et al., 2012), eustatic sea level rose relatively quickly (Lambeck et al., 2014), and the Bengal shelf experienced a major transgression that permitted the shoreline to move ~250–300 km landward of its lowstand position at the Last Glacial Maximum (Waelbroeck et al., 2002; Palamenghi, 2012). On the delta plain, rapid sedimentation during the transgression buried the paleosol that had developed on the interfluves of the lowstand drainage system (Hoque et al., 2014). The climatic change also reinvigorated the monsoon, which had been suppressed during glacial times, yielding early Holocene sediment loads at least twice that of the present day (Goodbred and Kuehl, 2000a; Goodbred, 2003). The delta began to aggrade and prograde at this time (Goodbred et al., 2003, 2014), 2–3000 yr earlier than most other deltas. This indicates that sediment supply was sufficient to keep up with the accommodation (Fig. 2) generated by rapid eustatic sea level rise. During the mid Holocene (~7 kyr ago), the rate of sea level rise slowed an order of magnitude. The delta shoreline trajectory shifted from more aggradational to highly progradational, advancing the shoreline about 100 km seaward of maximum transgression and the delta front of the subaqueous clinoform ~200 km farther seaward (Kuehl et al., 2005; Palamenghi, 2012). It is currently prograding at 12–15 m/yr (Michels et al., 1998).

The distribution of sediment supply over the delta differed between the aggradational and progradational phases. More sediment was trapped farther upstream in the alluvial and coastal plains during aggradation than during progradation (Goodbred and Kuehl, 2000b; Cattaneo and Steel, 2003). Also, during the early Holocene, glacial lake outburst floods (Montgomery et al., 2004) may have further excavated the glacial valleys that were cut during the lowstand (Pickering et al., in press). In contrast, channel migration and avulsions in the fluvial plain appear to be more important during the mid-late Holocene than during early Holocene when rivers were confined to their deep glacial valleys (Pickering et al., 2014; Sincavage et al., in press).

2.2. Morpho-tectonic setting

The GBMD can be divided into several tectonomorphological units. There is evidence of active tectonics in the eastern and northeastern part of the GBMD. To the east, the delta transitions to the Indo-Burma foldbelt, which overthrusts the thick sediments of the Bengal Basin (Fig. 1). The eastern delta overlies this tectonically active foldbelt that has been buried by deltaic sediments during the current highstand (Steckler et al., 2008). We use the westward extent of the deformation front as mapped by Steckler et al. (2016) as the limit of the eastern delta that overlies the tectonically active foldbelt. In the northeast, the delta is overthrust by the Shillong Massif, bounded by the Dauki fault system that may represent the beginning of a forward jump of the Himalayas (Vernant et al., 2014). In the west, the delta onlaps against the Indian craton (Lindsay et al., 1991; Steckler et al., 2008). The northwestern limit of the delta is less clearly defined.

The northern and western sides of the delta cover a feature termed the “Hinge Zone” that represents the position of the Eocene shelf edge and the transition from the Indian craton to thinned crust across a Cretaceous passive margin (Lindsay et al., 1991; Talwani et al., 2016). The depth to crystalline basement drops and the crust thins (Singh et al., 2016), eventually transitioning to oceanic crust to the southeast (Figs. 1 and 2). Its role regarding the subsidence pattern in the modern delta is uncertain.

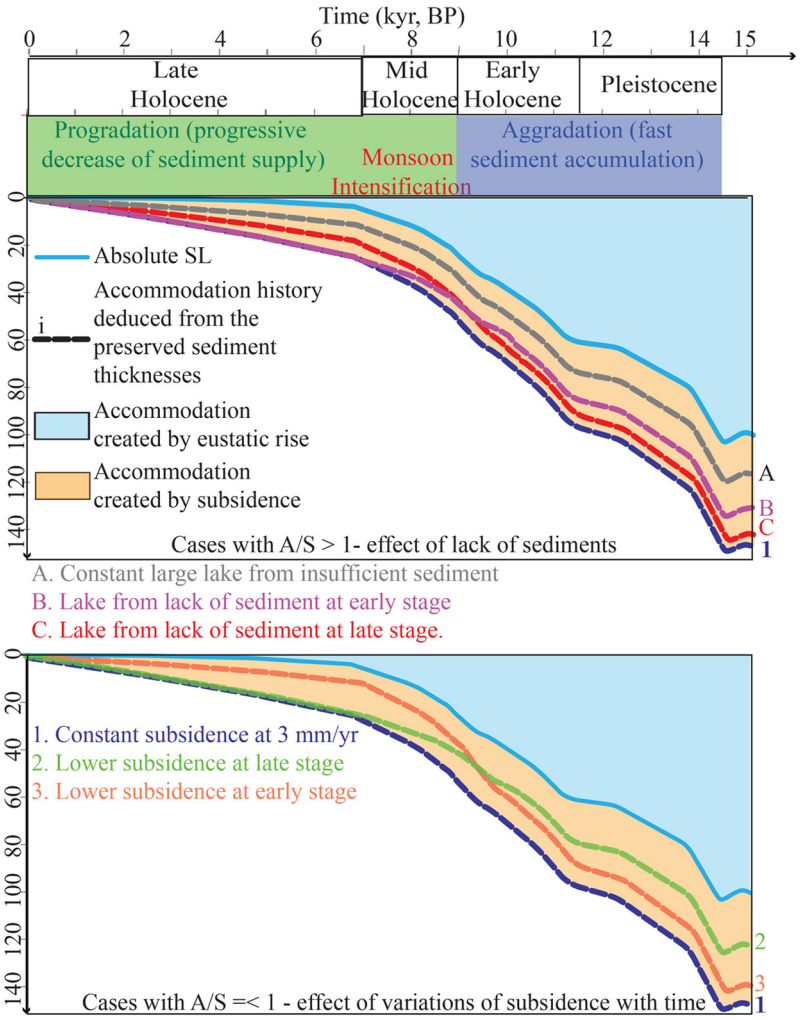

Fig. 1. Conceptual representations of the stratigraphic base-level approach used in this study through the Holocene sea-level rise history. The accommodation history deduced from preserved sediment thicknesses (in thick dashed lines) may represents the Relative Sea-Level (RSL) history only if sediment supply is enough high to fill the accommodation ($A/S \leq 1$, bottom graph). In this case, the RSL history represents the summation of the local absolute sea level (in blue) and subsidence (in orange). The simplest case (1, in blue) represents the RSL for a constant subsidence rate of 3 mm/yr, while cases 2 and 3 represent the RSL if subsidence changes through time. Cases A, B and C (top graph) represent the accommodation history deduced from preserved sediment thicknesses if sediment supply is not high enough to fill accommodation ($A/S > 1$) during the entire Holocene (A) or during parts of the Holocene (B and C). In these cases, the RSL cannot be deduced from the accommodation history. Also, the three main periods that the GBMD experiences over this period are represented: (1) the early Holocene aggradational period, (2) the mid-Holocene Monsoon Intensification with greater sediment supply and (3) the late Holocene progradational period. The eustatic curve represented in this figure and in other figures is the global eustatic curve from Lambeck et al. (2014). (For interpretation of the colors in the figure(s), the reader is referred to the web version of this article.)

Within the nontectonic part of the delta, we distinguish between the upstream fluvial fan delta and the downstream fluvial-tidal delta (Wilson and Goodbred, 2015). They form two distinct morphological domains with river slopes differing by an order of magnitude between the fluvial fan delta ($\sim 10^{-4}$) and the fluvial-tidal delta ($\sim 10^{-5}$). The channels in the fluvial fan delta are predominantly braided streams that undergo rapid channel aggradation and lateral migration. In contrast, channels in the fluvial-tidal delta are more stable and undergo progressive bifurcation downstream (Wilson and Goodbred, 2015). Thus, we divide the GBMD into four morphotectonics domains (Fig. 1).

3. Data acquisition and processing

3.1. Tube-well dataset

More than 400 hand-drilled tube wells have been collected over the GBMD as part of the BanglaPIRE project (Goodbred et al., 2014; Pickering et al., 2014). The sampling strategy consists of transects of tube wells spaced 3–5 km across the delta (Pickering et al., 2014; Sincavage et al., in press, Fig. 1) with a target depth of the top of the Pleistocene to recover the complete Holocene stratigraphy. This dataset has been used to map the depth of the Pleistocene over the delta (Sincavage et al., in press, Fig. 1). In each well, samples were obtained every 1.5 m and more than 18,000 sediment samples have been collected. Systematic grain size analyses (laser-diffraction particle size analysis) and X-ray fluorescence (XRF) have been carried out on samples (Sincavage et al., in press). Stratigraphic logs were made with the same 1.5 m resolution.

Geochronology was obtained from radiocarbon analyses on organic matter samples, primarily wood with some grass and leaf fragments. Three ages were also collected on well-preserved gastropod shells. Samples were recovered from a variety of sedimentary facies, including channel and bar sands, and flood plain and tidal plain muds (Supplemental Material 2). However, as peats and datable material from basal flooding surfaces are rare in the GBMD, few of the samples from the current database can be considered as sea-level index points with a high indicative meaning, such as those normally preferred for sea-level reconstruction (e.g., Shennan, 2007). In this case we consider each radiocarbon sample in

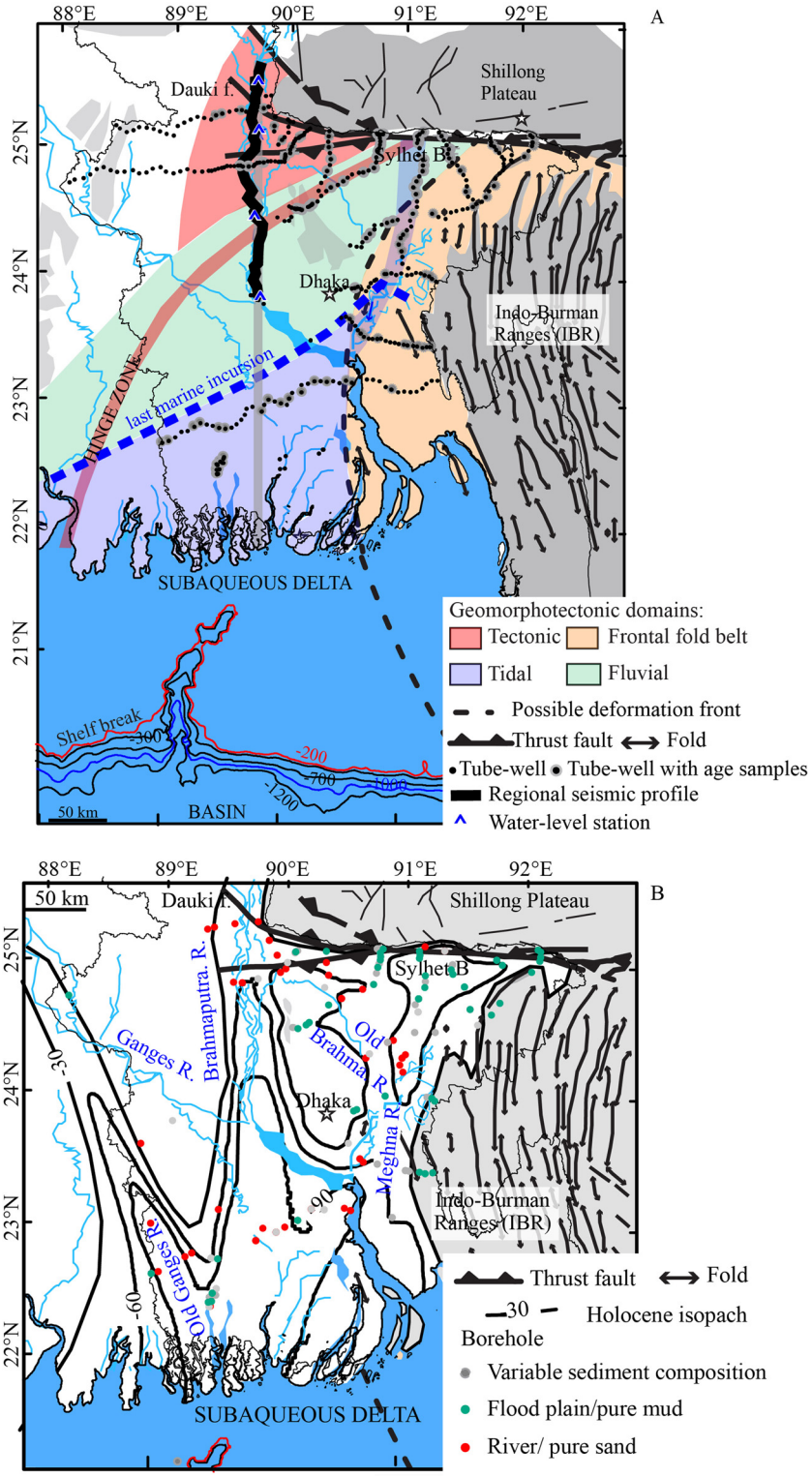

Fig. 2. A. Geomorphotectonic domains of the GBMD and data distribution. The delta is overthrust by the Shillong Plateau and the Indo-Burman foldbelt, respectively, to the north and east. The Hinge Zone is defined as the inherited passive margin limit, i.e., the edge of the Indian Craton (from Alam et al., 2003). Two tectonic domains are represented: (1) the frontal part of the fold belt (in orange), which is represented as in Steckler et al. (2016) and (2) the Dauki Fault system domain in red. The non-tectonic parts of the delta can be divided in two domains: the southern tidal (in blue) domain (Wilson and Goodbred, 2015), which corresponds to the backwater zone, and the northern fluvial dominated environment (in green). We note that this boundary closely follows the maximum extent of the last marine transgression during the Holocene (Sincavage et al., in press). B. Holocene main river paths superimposed on the Holocene isopach. The Holocene isopachs are obtained by a simple interpolation of all tube-well data (Sincavage et al., in press). Note how the Holocene isopachs follow the river channel paths, suggesting that sediment accumulations are higher in river channels than flood plains. Tube-wells are classified with respect to the grain-size of Holocene sediments and their distribution regarding the main river pathways. 3 categories of tube-wells are defined: (1) River channel data (in red) are located on main river pathways and sediments are almost pure sand over the entire Holocene section (sand content >75%). (2) Flood plain data (in green) are located in flood plain and sediments over the entire Holocene section are almost pure mud (sand content <25%). (3) Mixed environment data (in gray) present lithological logs where sand and mud alternate (sand content ranging 25%–75%) over the Holocene section.

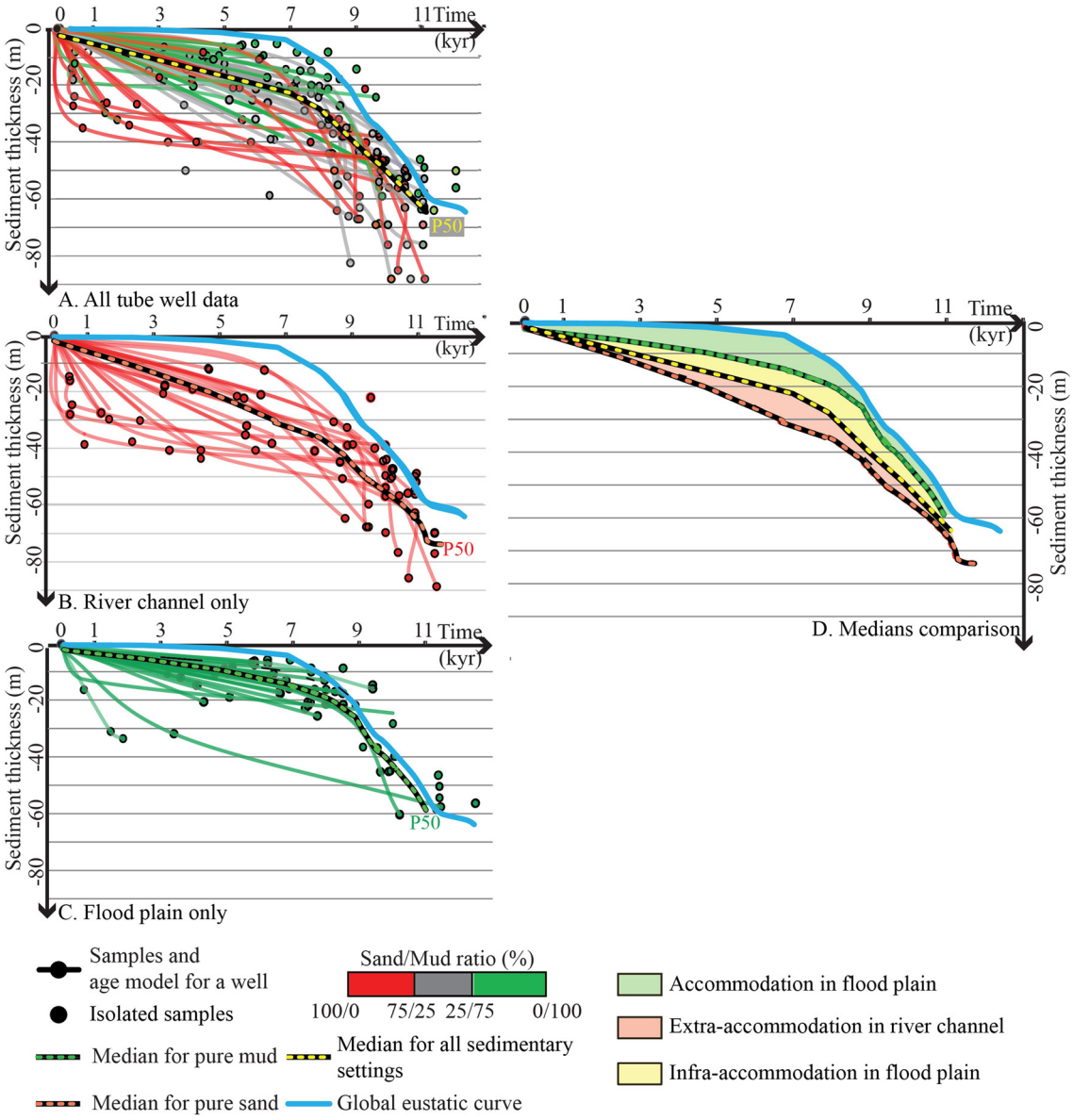

Fig. 3. Statistical analysis of the variability of the Holocene preserved sediment thicknesses with respect to the sedimentary environment. Tube-well data and sediment accumulation trends at each individual well are classified with respect to their locations relative to river channel pathways and their sediment grain-size (pure sand in red and pure mud in green, Fig. 1). Lines show age models for wells with multiple dates. The median (*P*50) of the preserved sediment thicknesses are calculated for pure sand (B), pure mud (C) and for all the tube-well data (A, used as a reference) every 1000 years. Differences in the cumulative preserved sediment thicknesses sediment for each case (D) are used as a proxy of the effect of the sedimentary variability on the sediment accumulation and to estimate the averaged accommodation from preserved sediment thicknesses (Fig. 4).

context of its associated facies, for example recognizing that samples from fluvial sands are likely from channels that incised below sea level in much of the lower delta plain.

All radiocarbon ages were measured by accelerated mass spectrometry (AMS) at the National Ocean Sciences Accelerator Mass Spectrometry facility (NOSAMS, at the Woods Hole Oceanographic Institution). Ages obtained were calibrated using *Calib* software and are reported in sidereal years from the calibrated radiocarbon dates (after Stuiver and Reimer, 1993). A total of 198 ages have been determined and they allow us to place constraints on sediment accumulation rates at 96 sites. This large dataset enables us to perform some statistical analysis, with the limitation that the dataset is heterogeneously distributed over the different morpho-tectonic domains. The sampling is not dense enough in either of the two tectonic domains (the Dauki Fault system and the frontal part of the foldbelt, Fig. 1) to properly determine the high spatial variability of subsidence in these two domains. In the fluvial domain, most of the tube well data come from the northeastern part of the domain, the Sylhet Basin (Figs. 1 and 3). Farther west, the regional seismic profile acquired along the Jamuna–Brahmaputra River provides additional insights about subsidence in both the tectonic and the fluvial domains.

3.2. Multi-channel seismic reflection and correlation between well data and multichannel seismic reflection

A 255-km long very high resolution seismic profile along the Brahmaputra–Jamuna River has been constructed by combining 6 shorter seismic profiles acquired along the river (Fig. 7, Pickering et al., in press). The longitudinal profile crosses the tectonic and the fluvial domains along the Jamuna braidbelt. Seismic data were collected using a very high resolution marine multichannel system (single 0.1L GI Gun source towed at 1 m depth used with a short 50 m streamer of 48 hydrophones also towed at 1 m depth)

during the flood season (Pickering et al., in press). Post-acquisition processing was performed to increase the signal to noise ratio and improve poor imaging associated with shallow water conditions, complex navigation tracks and motion of the streamer in the water column. The processing has been carried out by using Schlumberger Vista and the data analysis by using IHS Kingdom software (Pickering et al., in press). A series of corrections (including the water elevation changes along the river) was done to aid the analysis of the geometry of the sedimentary reflectors identified in the profiles (Pickering et al., in press).

The two main sedimentary reflectors (the riverbed and the last main unconformity) were mapped in the time domain. Results were subsequently transformed in the depth domain (by using a constant average velocity of 1480 m/s for the water and 1550 m/s for the interval between the riverbed and the last main unconformity, Pickering et al., in press). The profiles of these two reflectors were projected along a simplified navigation track that follows a N–S trending line (using GMT), in order to simplify the geometry and obtain interpretable slopes of sedimentary reflectors. Seismic horizons were correlated to strata identified in the lithology logs of both our tube wells and preexisting geotechnical borings from the Jamuna Bridge feasibility study (JICA, 1976). The physical property measurements determined at the JICA-S1 well (JICA, 1976) were used to calculate a synthetic seismogram with the same frequency content as the seismic signal (supplemental material 1). This seismogram was compared to the seismic traces in order to confirm the correlation between the sedimentary units and the seismic signal. The main unconformity corresponds to a gravel bed obtained at both river crossings that had been excavated 10,000 years ago. This unconformity is thus named the last glacial lowstand incision surface of the river (Pickering et al., in press).

4. Base-level stratigraphic method developed in this study

4.1. Principles and challenges

Stratigraphically, the sediment deposition on a continental margin depends on the space available (the accommodation) with respect to a base level that is considered in this study to be the relative sea level (Schumm, 1993; Penland and Ramsey, 1990). More precisely, the infill of sediment deposited below the base level represents the balance between the accommodation (A) (created primarily by both eustatic rise and subsidence) and the sediment supply (S) that fills it (A/S ratio, Barrell, 1917; Wheeler, 1964; Neal and Abreu, 2009; Fig. 2).

In a channelized system, variation in accommodation (A) is not only the result of the eustatic sea level and subsidence. Indeed, surface processes also play a role in creating accommodation (Nittrouer et al., 2012) as rivers erode below base level seaward of the backwater limit. During periods of sea level rise, the increasing base level may cause valleys to backfill leading to higher depositional rates than on the flood plain (Schumm, 1993; Catuneanu, 2006). This explains the pattern of the isopach map of the Holocene section (Sincavage et al., in press), that is strongly influenced by the locations of the major lowstand valleys of the Ganges, Brahmaputra, and Meghna Rivers (Fig. 1). Thus, differences in the filling of accommodation between flood plain and river environments must be considered when interpreting the preserved stratigraphic record to obtain a correct estimation of accommodation and associated subsidence.

4.2. Approaches developed in this study

We are using three different and independent approaches to estimate the Holocene accommodation pattern and history over the GBMD from the preserved sediment thicknesses. First, we analyze the variability in the preserved sediment thicknesses as a function of the sedimentary environment, which is defined by considering the Holocene river occupation history during the Holocene (Sincavage et al., in press; Fig. 1) and the sediment properties. Tube well lithological descriptions and sediment grain size analyses are used to defining a sand/mud ratio (calculated as the percentage of sand between two samples) for each individual sample. This approach enables us to identify all wells that sit exclusively in a pure muddy flood plain environment and exclusively in a sandy channel environment over the entire Holocene. Those two end-member series are statistically analyzed to determine a factor that represents the average variability of the accumulation in a channelized system compared to the unconfined estuarine and deltaic plains. In addition, this factor may also incorporate differences in preservation potential associated with the different sediment environments. However, since our estimates are based on the analysis of empirical data, we cannot quantitatively determine the relative importance of each individual process.

This factor is primarily applied to the Holocene isopach map and thus derive from it a regionally averaged pattern of accommodation. Once the isopach is averaged, a gently seaward gradient in accommodation can be derived from the smoothed Holocene isopach. Secondly, the averaged accommodation history is statistically determined for each geomorphological domain. Results obtained also suggest a seaward increase in accommodation. The averaged seaward gradient that we determine is then used to analyze the Holocene accommodation history. Finally, we reconstruct the burial history of the last glacial lowstand incision surface of the Brahmaputra River imaged on multichannel seismic reflection profiles. A N–S seaward gradient in accommodation is also obtained by this approach.

N–S seaward gradient in accommodation obtained by these three different approaches are then compared together. The three different seaward gradient estimates converge, thus we combine these results to compute a map of the distribution of the accommodation over the Holocene. As the variability in accommodation associated with the sedimentary environment has been taken into account in these three analyses, we conclude that the averaged accommodation represents the local eustatic rise and the additional accommodation associated with subsidence.

Constrains on the local eustatic curve are scarce in the region, thus we assume the accommodation created by the eustatic rise follows the global eustatic curve. The reconstructions of the pattern of the sediment accumulation for tube-well data that have sufficient samples follow the trend of the global eustatic rise (Fig. 3). This suggests that the assumption that the sediment accumulation is controlled, to the first order, by the global eustatic rise with coeval subsidence is a valid working hypothesis. However, we recognize that the Bengal Basin is a far-field relative sea level region (Khan et al., 2015; Milne and Mitrovica, 2008) and thus while the local sea-level may be slightly above the global eustatic sea-level during the mid-Holocene (aka the mid-Holocene highstand), the eustatic curve is close to local sea level. Our approaches are relative, and sites are considered as a group. As a consequence, approximating the local absolute sea level with the global eustatic one should not alter the quality of results. Also, our analyses are based on the stratigraphic hypothesis that the A/S ratio is <1 throughout the Holocene (Fig. 2). This is consistent with the high rate of early Holocene (7–11 kyr) sediment supply, and the limited marine transgression and the early start of progradation of the GBMD during the Holocene relative to other deltas (Goodbred and Kuehl, 2000a; Goodbred et al., 2003).

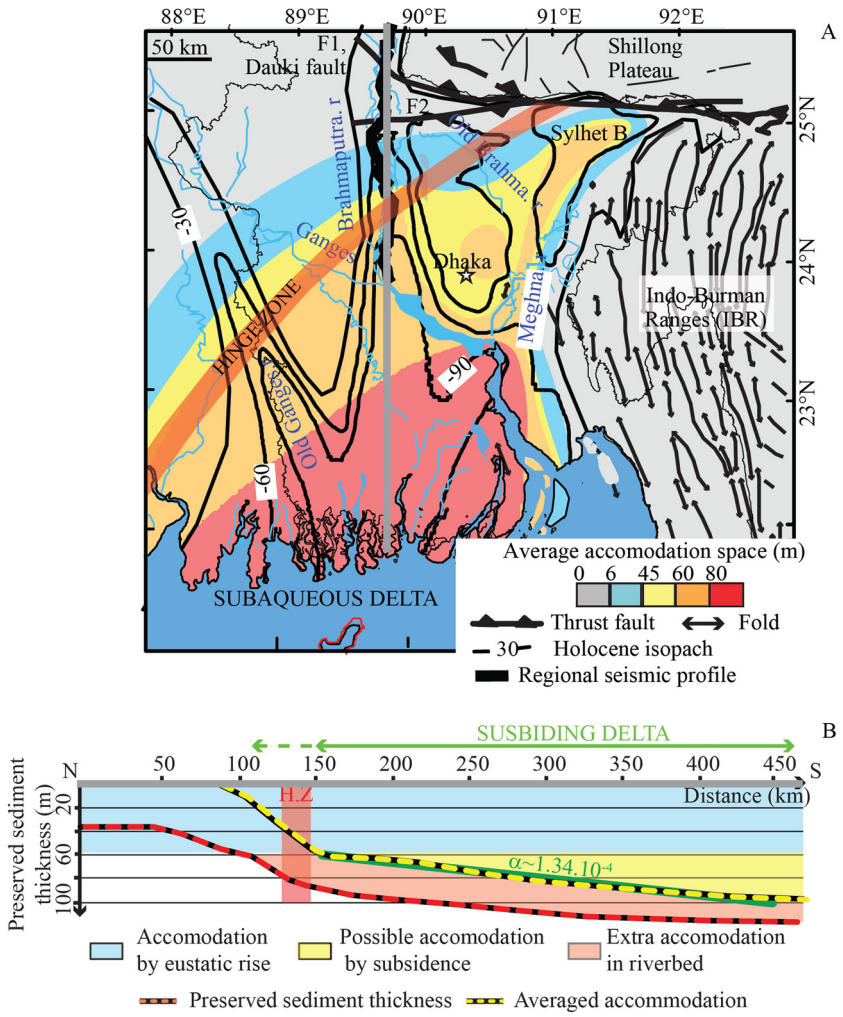

Fig. 4. Preserved Holocene sediment thicknesses superimposed on the Holocene averaged accommodation space and averaged seaward gradient in accommodation. A. The Holocene averaged accommodation space is obtained by taking into account the variability associated with the sedimentary environment on the preserved sediment thicknesses (Fig. 3). B. Comparison between the Holocene preserved sediment thickness and averaged accommodation along a N–S profile and seaward gradient in accommodation. The boundary of the subsiding domain is estimated by calculating the area where the average Holocene accommodation is higher than the 60 m of accommodation related to the eustatic sea-level rise.

5. Results

5.1. Estimation of the variability in accommodation between river channel and averaging the Holocene isopach

We define 3 different categories of tube well data according to the sand/mud ratio computed for each individual samples and the location of tube-wells relative to the Holocene river occupation history (Sincavage et al., in press; Fig. 1). All samples located within the Holocene main river pathways containing a proportion of sand higher than 75% (in red, Figs. 1 and 3) are considered to be a sandy environment representing deposits in a river channel. All samples that have a sand ratio lower than 25% (in green, Figs. 1 and 3) and collected outside of the main Holocene river pathways are considered to represent deposits in the flood plain. Samples with a ratio ranging between 25 and 75% (in gray, Fig. 1) are considered as mixed-environments. In those cases, the Holocene sections logs consist of mud alternating with channel sand deposits and thus the mud may have been deposited in either an abandoned channel or in a flood plain. Thus, at those wells, we acknowledge that we cannot completely resolve the effect of the sedimentary environment on the geological archive.

All wells, that sit exclusively in a pure flood plain environment (Fig. 3A) and exclusively in a channel environment (Fig. 3B) within any geomorphological domains (with the exception of the fold-belt domain), were plotted together to yield a sufficient number of samples (59 sand samples for 56 mud samples) to be considered statistically representative. For each category, we compute the median of the accommodation filled by each series (sand vs. mud). We also computed a global accommodation curve by considering the median of all samples together (regardless their sedimentary environments) to use as a reference (Fig. 3C). Comparison of the median curves suggest that the accommodation in a pure river channel is higher by up to 35% compared to the global accommodation curve whereas the accommodation in pure flood plain is lower by 15% compared to the averaged pattern (Fig. 3C). We use this value as an average representation of the variability in the preserved sediment thicknesses in a channelized system compared to the unconfined estuarine and deltaic plains. We use these estimates of variability in preserved sediment thicknesses for defining a smoothing factor of the Holocene isopach (Fig. 4). This factor is used to average the accommodation pattern over the delta. Thus, the averaged accommodation in river channel is 35% of the preserved sediment thicknesses and 15% in flood plain environment (Fig. 4). The map obtained (Fig. 4) shows a gentle seaward gradient in accommodation over the deltaic margin, of $1.34{\cdot}10^{-4}$ (Fig. 4C) in the N–S direction.

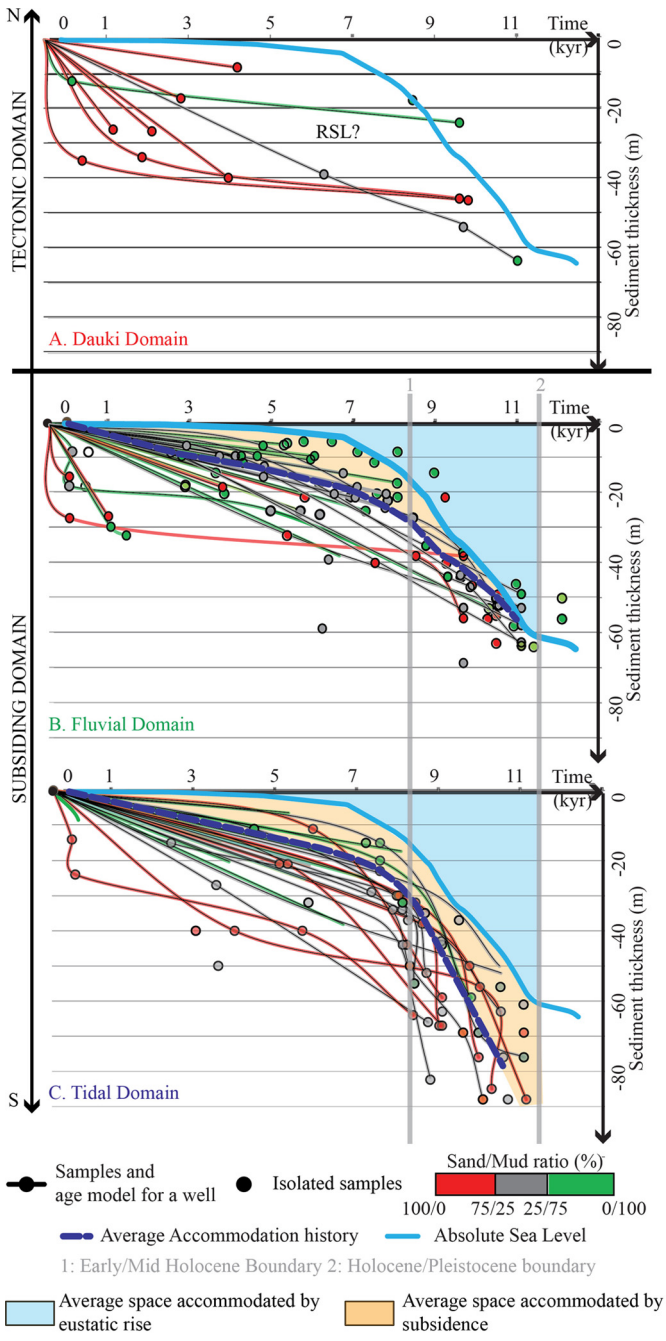

Fig. 5. Averaged accommodation history and associated subsidence determined by analyzing tube-well data according to their geomorphological domain (Fig. 1A). Age model and sediment accumulation histories are shown for each individual well. No clear pattern of accommodation can be identified in the Dauki domain (A). The data are limited, scattered, and the preserved sediment thicknesses appear strongly influenced by fluvial and/or tectonic processes. Averaged accommodation history and subsidence are determined for the fluvial (B) and tidal domains (C). The same color code as in Fig. 3 is used to represent the grain-size (sand/mud ratio), as a proxy of the sedimentary environment.

5.2. Analysis of the variability on preserved sediment thicknesses by geomorphological domain

We reconstruct the accommodation history from the preserved sediment thicknesses in the tidal and the fluvial domains, the two geomorphological domains where the numbers of tube-well data are sufficient to be considered as statistically representative (Fig. 5). However, pure sand and pure flood plain samples are not large enough to be examined separately for each geomorphological domain. Thus, we do not examine them separately, but group the different environments (river, flood plain and mixed), which are almost equally represented in the dataset. Thus, the median of all the dataset for each geomorphogical domains, regardless the sedimentary environments, should represent the average pattern (Fig. 5). The amount of accommodation that may be associated with subsidence is significantly higher in the tidal domain than in the fluvial domain over the entire Holocene (Fig. 5). In the tidal delta plain, the accommodation appears to be created at almost constant rate over the entire Holocene. In contrast, in the fluvial domain, the creation of accommodation appears to be lower during the early Holocene than during the later periods of the Holocene. Most of the tube-well data in the fluvial domain are collected in the northern part of this domain, from the Sylhet Basin. It has been suggested that the sediment input in this area is reduced during the early Holocene, as the Brahmaputra flowed down the Jamuna pathway and limited sediments entered the Old Brahmaputra pathways (Sincavage et al., in press). Thus, this apparent decrease of accommodation may be explained, or partially explained, by a lower rate of sediment deposition in this part of the fluvial domain. The Sylhet Basin is underfilled during this time period and the accommodation is higher than the sediment supply during the early Holocene. By the mid-Holocene, the Brahmaputra avulsed eastward into the Old Brahmaputra valley (Goodbred and Kuehl, 2000a; Pickering et al., 2014; Sincavage et al., in press), allowing backfilling of the Sylhet basin and an environment where sediments are better distributed over the delta. From this time onwards, the accommodation appears to evolve with the same pattern in both domains (Fig. 5). We thus computed the seaward gradient of accommodation since 8.2 kyr (Fig. 6A) and since the Pleistocene/Holocene transition (Fig. 6B) and obtained values of 1.0 and $1.1 \cdot 10^{-4}$ respectively. This confirms the seaward gradient in accommodation previously obtained by smoothing the Holocene isopach (Fig. 4). This result will be further evaluated by comparing it with the burial history of the seismically imaged buried unconformity.

5.3. Seaward gradient on accumulation from the burial history of the last glacial lowstand incision surface of the Brahmaputra river

Present-day slopes of both the modern riverbed and the buried seismically-imaged last glacial lowstand incision surface unconformity have been determined by projecting the seismic data along a N–S profile. Both the riverbed and the unconformity have a significant roughness and shortwave-length variations; the best correlation coefficient is obtained by a linear regional trend along these two surfaces that may be indicative of the regional slope. The gradient of the modern riverbed and water surface slopes (Fig. 7B, $0.7 \cdot 10^{-4}$) are five times lower than the gradient of the buried unconformity (Fig. 7B, $3.6 \cdot 10^{-4}$). It is inferred from this difference that part of the present slope of the unconformity is likely due to its differential subsidence and burial history.

Since the buried unconformity possibly had a different slope than the current river when it was at the surface, it is necessary to estimate what the paleoslope of this surface might have been, in order to use it at a reference for analyzing the subsidence and sediment accumulations. We therefore compute using empirical laws (Trampush et al., 2014; Li et al., 2015) the possible range of equilibrium slope of the Jamuna–Brahmaputra River as a function of the average flow depth (H) and the grainsize of the suspended (D_{50}) and the basal (D_{95}) loads (see supplemental material for calculations). The range of values we estimate for both the Holocene and Pleistocene Brahmaputra is comparable with the observed modern river slope (Fig. 7B, $0.7 \cdot 10^{-4}$), as well as the present water surface gradient, but it is significantly lower than the present day slope of the low-stand unconformity (Fig. 7B, $3.6 \cdot 10^{-4}$).

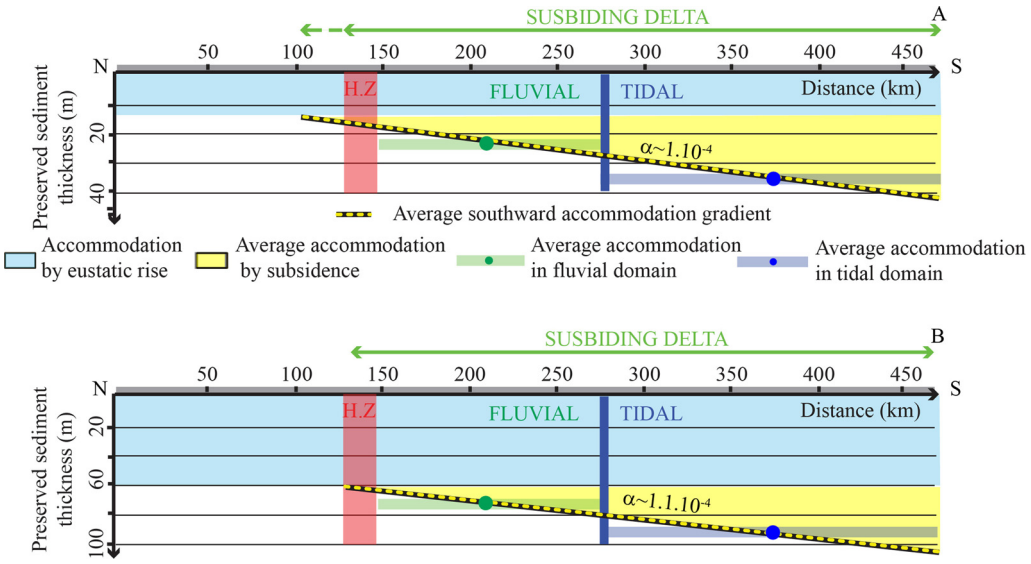

Fig. 6. Gradient in accommodation projected along a N–S line obtained by analyzing tube-well data by geomorphological domain (Fig. 5). A. Gradient obtained by considering accommodation since the Early/mid Holocene boundary (Fig. 5, time limit 1). B. Gradient obtained by considering the accommodation since the Holocene/Pleistocene boundary (Fig. 5, time limit 2).

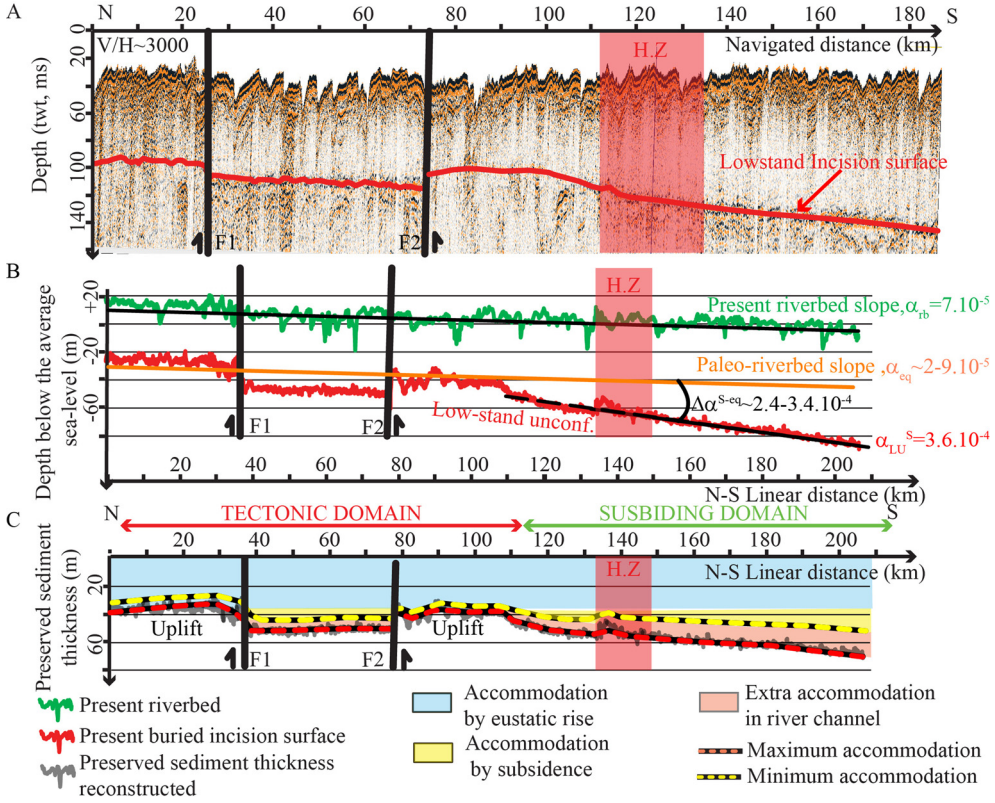

Fig. 7. The seismically imaged last glacial lowstand incision surface of the Brahmaputra river and reconstruction of its burial history and associated subsidence pattern. A. Composite regional seismic reflection line that images the last glacial lowstand incision surface. The surface has been correlated to borehole data (see supplemental material) and its age estimated accordingly (10 ka, see Pickering et al., in press). The surface is offset by two faults (F1 and F2, in the Dauki fault system domain) and dips seaward south of the Hinge Zone indicating subsidence of the Bengal Basin (subsidence domains). The location of the composite regional seismic profile can be founded on the Figs. 1A, 4 and 9. B. N–S projection of the horizons mapped along the seismic profile (the present riverbed and the buried incision surface) and analysis of their slopes (annotated α. The possible paleo-slopes of the lowstand unconformity is empirically estimated (Table 1 in supplemental material, αS_{eq}) and used to reconstruct the slope of the buried lowstand unconformity (residual slope annotated $\Delta\alpha S_{eq}$). C. Estimation of the accommodation associated with subsidence created since the last glacial lowstand incision surface. The residual slope of the incision surface i.e., corrected by its paleoslope) is used for estimating the seaward gradient in subsidence during its burial history. The subsidence is estimated by subtracting the cumulative space created by the Holocene eustatic rise and correcting for the variability in preserved sediment thicknesses of the sandy channel (Fig. 4).

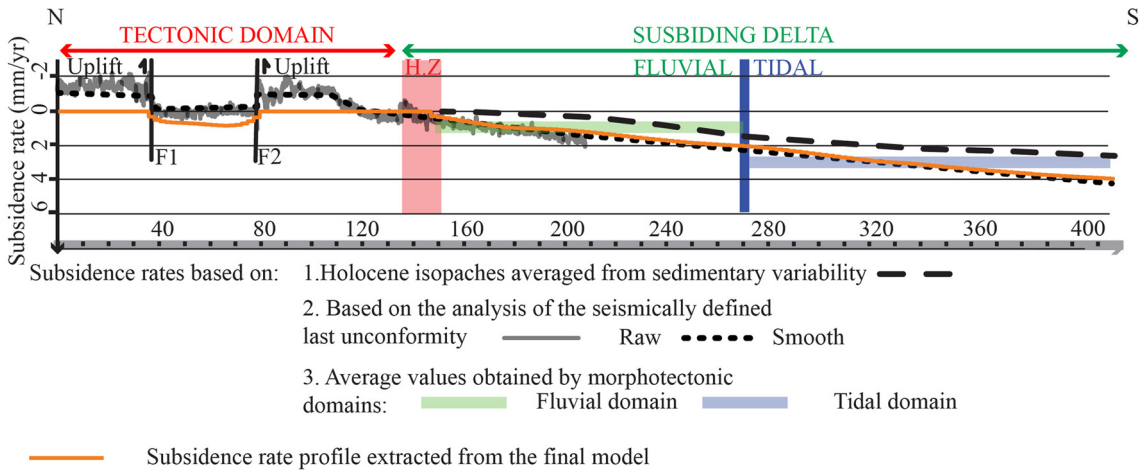

Fig. 8. Comparison of subsidence rates obtained by considering results on accommodation obtained from the three different approaches developed in this study (see Figs. 4, 6 and 7). Subsidence rates are given along a N–S profile (see Fig. 9 for the location of the profile). The subsidence rate extracted from the final map of subsidence presented in Fig. 9 is also projected along the same N–S line.

During the early Holocene, the Brahmaputra incised valley may have been excavated and widened by high discharges from glacial lake outburst floods upstream (Montgomery et al., 2004) that were capable of transporting the cm-scale gravel observed at the base of the valley (Pickering et al., in press). As a consequence, sediment load might have been twice as high during the early Holocene compared to the modern load (Goodbred and Kuehl, 2000a). Consideration of the possible variations in river discharge and flow depth suggest about a factor of 2 variability of the paleoslope relative to the modern river slope (i.e., $0.7 \pm 0.5 \cdot 10^{-4}$, named α_{eq} on Fig. 7). The present slope of the unconformity has therefore been corrected by this range of values, and we obtained a residual gradient in accommodation of 2.4 to $3.4 \cdot 10^{-4}$ (Fig. 7). This gradient corresponds to the sandy river channel environment, therefore we reduce the gradient by the 35% excess subsidence seen river channels to $1.6\text{-}2.2 \cdot 10^{-4}$, slightly higher than the gradients obtained by using tube-well data.

6. Results integration and construction of a subsidence map

We are using the average seaward gradients in accommodation to construct a map of the subsidence over the GBMD (Fig. 10). The mean of the three gradients is $1.3\text{–}1.6 \cdot 10^{-4}$ along a N–S direction. The gradient obtained by reconstructing the burial history of the last glacial lowstand incision surface of the Brahmaputra river is slightly higher (1.6 to $2.2 \cdot 10^{-4}$) than the gradient obtained by analyzing the tube-well data (between 1 and $1.34 \cdot 10^{-4}$). The sediment thickness and age of the preserved sediments in the Jamuna–Brahmaputra riverbed were possibly modified by additional channel incision during the Holocene, particularly during the early Holocene glacial lake outburst floods. The incision would have eroded roughly a channel depth of sediment, which would then be filled by younger deposits altering the apparent sediment accumulation. The incision might range between 0 and 25 m (Reitz et al., 2015). This could possibly explain the slightly higher N–S gradient in accommodation that we obtained here compared to the values obtained by analyzing the tube-well data.

Assuming that the delta is at or near base level over the entire Holocene, we infer that subsidence must have occurred where accommodation is greater than the space created by eustatic rise. Results from the three independent approaches suggest that the accommodation is equal to the value of space created by eustatic rise at the Hinge Zone (Figs. 4 and 6B) or perhaps 20 km north of it (Figs. 6A and 7). This suggests that subsidence is close to zero at the Hinge Zone and that subsidence plays a role in the growth of the delta south of it. Thus, the Hinge Zone can be viewed as the close to the northern limit of the subsiding delta (Figs. 4, 6 and 7). Is has been showed that the Hinge Zone represents the transition from the Indian craton to a thinned crust or an oceanic crust (Lindsay et al., 1991; Talwani et al., 2016; Singh et al., 2016). The contrast between the thick Indian craton and the transitional to rifted and oceanic lithosphere should correspond to changes in the subsidence between these two regions. However, the thermal subsidence of this older passive margin should be small (Stein and Stein, 1992). In contrast, the flexural rigidities across the margin are expected to be considerably different, affecting the flexural component of subsidence (Lavier and Steckler, 1998; Burov and Molnar, 2008) and localizing bending of the basin at the transition (Waschbusch and Royden, 1992). This may explain why this inherited structure marks the northern limit of the modern subsiding delta. The variability of 20 km on the location of this limit may represent the uncertainty on the location of the Hinge Zone which has been defined only according to few control points along multichannel seismic profiles (Lindsay et al., 1991) and, as the result, the Hinge Zone location differs between studies (e.g., Lindsay et al., 1991 vs. Singh et al., 2016). Furthermore, Steckler and ten Brink (1986) show that the weakest lithosphere occurs slightly landward of continental margin hinge zones.

The subsidence map has been constructed by considering the Hinge Zone as the subsidence onset zone (<0.2 mm/yr) and using the seaward gradient of accommodation that we determine to constrain the subsidence pattern. For the subsiding delta domain, the distribution of subsidence is primarily derived from the averaged accommodation pattern obtained accordingly to the smoothed Holocene isopach, which suggests that the maximum seaward gradient has a NW–SE strike. Then, the different gradient values obtained along a N–S direction by the three different approaches are used to estimate uncertainty on the subsidence values (Fig. 8). Seaward of the Hinge Zone, subsidence increases to ~2 mm/yr across the fluvial delta (Fig. 8 and Fig. 9). Farther to the SE in the tidal delta, subsidence rates increase to >4 mm/yr, reaching a maximum of ~5 mm/yr near parts of the coast (Fig. 9). East of the Meghna River, the delta overlies the buried front of the IndoBurma accretionary prism. Subsidence rates decrease and transition to uplift in the exposed IndoBurma foldbelt.

Tube-well data are insufficient to constrain the pattern of subsidence in the tectonic domain associated with the Dauki fault system (Fig. 6). Thus, we use the results from the reconstruction of the burial history of the last glacial lowstand incision surface of the Brahmaputra to provide a possible rate of subsidence in this

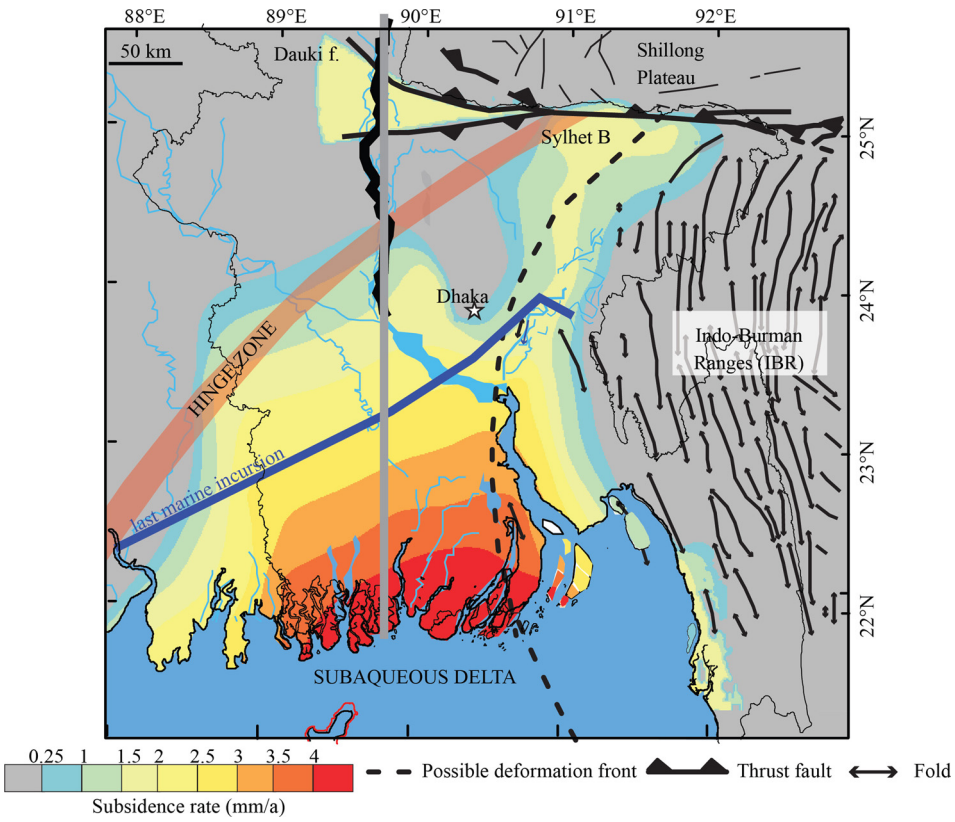

Fig. 9. Estimated distribution and rate of subsidence over the Holocene obtained by analysis of results from both seismic and tube well data. Subsidence shows a gradual seaward increase from the Hinge Zone marking the edge of the Indian craton. The subsidence rate in the Sylhet basin may be underestimated due to the underfilling of the basin.

domain. This result suggests the Dauki fault system produces both uplift and subsidence motions (Fig. 7). But, we recognize that we do not have any independent constrains for this domain, thus uncertainty about the subsidence rates in this domain has not been evaluated. Also, subsidence in the Sylhet Basin may be underestimated because of underfilling of this low elevation region, as suggested by the accommodation history observed in the fluvial domain.

7. Discussion and conclusion

7.1. The importance of considering the variability on preserved sediment thicknesses in the analyse of stratigraphic archives

Preserved sediment thicknesses are primarily related to the interplay of eustatic variations, subsidence and sediment supply. However, differences in the preserved sediment thicknesses between sites may also be related to other processes that are critical for elucidating the accommodation history and the associated subsidence from the preserved sediment archive. The sediments that fill the accommodation are brought by the rivers, and are distributed over the delta by fluvial branches which undergo avulsions and diversions. As a consequence, sediments are composed of stacks of channel/flood plain deposits, which are characterized by different deposition rates and sediment properties. This creates large spatial variability in the accommodation history that is related to fluvial processes. It also generates contrasting preservation potential between floodplain and channel deposits, as mud and sand compact differently during their burial histories (Revil et al., 2002). It is thus critical to consider these processes in the analysis of the preserved sediment thicknesses in order to obtain an accurate estimate of accommodation and subsidence.

Published subsidence rates in the GBMD are both scarce and scattered and are derived directly from the preserved sediment thicknesses, and thus suggest higher rates of subsidence in river channels relative to the fluvial plains (e.g., Brown and Nicholls, 2015). This is clearly an artifact and it is generally why most of indicative meanings of sea-level index points obtained outside of the tidal domain are considered low (Shennan, 2007). We developed a new simple statistical approach that aims to estimate the variability that requires only enough data to be statistically representative, i.e., >25 wells for each sedimentary environment. This approach has two main advantages. The first one is being able to estimate a spatially averaged regional pattern of subsidence that also characterizes the regional variability of subsidence. This is critical for modeling and better understanding the main driving forces that control the subsidence. The second advantage of this method is to provide absolute subsidence rates and sea-level index points that are averaged by morphotectonic domains. This can be viewed as an alternative method for defining SLIPs for environments out of the tidal domain. Thus, by using this method, average subsidence values can be estimated for other environments that are strongly influenced by rising sea-level. This method is exportable to other deltas plain, once the minimum amount of data necessary are acquired.

7.2. Significance of the subsidence pattern in the GBMD and comparison with other delta plains

We provide the first map of the subsidence pattern over the GBMD. The results show a gently increasing subsidence rate seaward of the Hinge Zone of the passive margin where the subsidence rates are <0.2 mm/yr to ~ 5 mm/yr at the toe of the subaerial part of the delta. The values appear to be moderate relative to other large deltas, such as the Mekong or the Mississippi

Delta (Anthony et al., 2015; Tornquist et al., 2008; Nienhuis et al., 2018).

One process that has been proposed to explain the high subsidence rates in deltas is sediment compaction (associated with both sediment dewatering and oxidation of organic material). This has been highlighted by a number of studies (e.g., Törnqvist et al., 2008; Horton and Shennan, 2009; Nienhuis et al., 2018; Karegar et al., 2015). In the GBMD, oxidation of organic material probably not as critical as some other deltas, such as the Mississippi or the Rhine–Meuse deltas, as pure peat deposits are significantly less widespread, primarily because of the large seasonal water table fluctuation and possibly from a lower organic matter concentration in sediments at depth (Neidhart et al., 2013). The mechanical compaction is a function of sediment properties (and notably the clay content, Revil et al., 2002) as well as the sedimentation rates (Grall et al., 2012). Variations in these parameters can drastically change the contribution of compaction. It is possible that sediment compaction is moderate in the GBMD, as the sedimentation is dominated by silty-sandy deposits with relatively low clay content. Together, these might explain the moderate rate of subsidence observed.

The map of subsidence that we obtained indicates a seaward gradient in subsidence rate. Such seaward gradients of subsidence are observed in most deltas, such as the Nile delta (Marriner et al., 2012; Stanley and Clemente, 2017; Gebremichael et al., 2018), the Mississippi Delta (Jankowski et al., 2016) and the Mekong delta (Anthony et al., 2015). This differential in accommodation in the seaward direction may have multiple causes. The seaward increase of sedimentation rates (Michels et al., 1998), as well as the increase of the amount of the fine fraction in the seaward direction can both drive a seaward increase of compaction. An increase in sediment thickness across the continental margin can also contribute to increasing compaction and subsidence in a seaward direction. Regionally, this gradient might be also related to the flexural response of the margin that possibly changes because of an increase of sedimentary loading in the seaward direction, and/or a seaward change in flexural rigidity (for instance from a transitional to an oceanic crust).

In many deltas, such as the Niger, Nile and the Mississippi deltas (Dokka et al., 2006) the margin shows evidence of gravitational collapse in the seaward direction, or the development of normal gravitational faulting along an efficient *décollement* layer, such as overpressured prodelta shales and/or salt. There is no suggestion that the seaward margin of the GBMD is collapsing, and unlike other deltaic margins its continental slope has a steep gradient (O'Grady et al., 2000). The depth of top of overpressure varies across the GBMD (Zahid and Uddin, 2005). However, in general, it is deeper than the shallow continental slope/rise break hindering the development of an effective *décollement*. Still, further analysis is necessary to better address this question.

The period of rapid Holocene sea-level rise also involved an increase of sediment input. The reinvigoration of the monsoon during the early mid-Holocene likely drove a pulse of sediment supply that exceeded double the present level (Goodbred et al., 2003). This temporal history of sediment loading should induce a viscoelastic isostatic response (Ferrier et al., 2015; Karpytchev et al., 2018) of the delta that helped drive the observed seaward gradient. Yet, it remains unlikely that the glacioisostatic response is a main factor that drives the Holocene subsidence. It may, however, contribute to a portion of the subsidence gradient. At this stage, it thus remains possible that the seaward gradient of subsidence and the moderate rates of subsidence may be related either to tectonic processes, to flexural and viscoelastic processes, to a moderate rate of sediment compaction, or a combination of these processes. A modeling effort is necessary to further address the relative importance of these various processes.

Most large deltas, lying at the interface of land and sea, are highly vulnerable to changing climate and sea level (Tessler et al., 2015). Yet, the hazard associated with the increase of relative sea level and associated subsidence may vary drastically from one delta to another. Results suggest that the GBMD is subsiding moderately under natural conditions. However, human intervention, such as groundwater withdrawal, the building of levees and embankments, and planned upstream dams and river diversion (Bagla, 2014) may increase subsidence or decrease the sediment accumulation in the GBMD placing the delta at further risk.

Acknowledgements

This project was supported by the U.S. National Science Foundation OISE 09-68354 and the Office of Naval Research N00014-11-1-0683. We acknowledge the NOSAMS Facility for the radiocarbon dating. We thank Nick Marriner, and an anonymous reviewer for constructive reviews. Lamont-Doherty Earth Observatory publication number 8235.

Appendix A. Supplementary material

Supplementary material related to this article can be found online at https://doi.org/10.1016/j.epsl.2018.07.008.

References

Alam, M., Alam, M.M., Curray, J.R., Chowdhury, M.L.R., Gani, M.R., 2003. An overview of the sedimentary geology of the Bengal Basin in relation to the regional tectonic framework and basin-fill history. Sediment. Geol. 155 (3–4), 179–208. https://doi.org/10.1016/S0037-0738(02)00180-X.

Anthony, E.J., Brunier, G., Besset, M., Goichot, M., Dussouillez, P., Nguyen, V.L., 2015. Linking rapid erosion of the Mekong River delta to human activities. Sci. Rep. 5.

Bagla, P., 2014. India plans the grandest of canal networks. Science 345 (6193), 128.

Barrell, J., 1917. Rhythms and the measurement of geologic time. Bull. Geol. Soc. Am. 28, 745–904.

Bern, C., Sniezek, J., Mathbor, G.M., Siddiqi, M.S., Ronsmans, C., Chowdury, A.M.R., Choudury, A.E., Islam, K., Bennish, M., Noji, E., Glass, R.I., 1993. Risk factors for mortality in the Bangladesh cyclone of 1991. Bull. World Health Organ. 71 (1), 73–78.

Brown, S., Nicholls, R.J., 2015. Subsidence and human influences in mega deltas: the case of the Ganges–Brahmaputra–Meghna. Sci. Total Environ. 527, 362–374.

Burov, E.B., Molnar, R., 2008. Small and large-amplitude gravitational instability of an elastically compressible viscoelastic Maxwell solid overlying an inviscid incompressible fluid: dependence of growth rates on wave number and elastic constants at low Deborah numbers. Earth Planet. Sci. Lett. 275 (3–4), 370–381.

Cattaneo, A., Steel, R.J., 2003. Transgressive deposits: a review of their variability. Earth-Sci. Rev. 62 (3–4), 187–228.

Catuneanu, O., 2006. Principles of Sequence Stratigraphy. Elsevier, Amsterdam. 375 p., ISBN-13: 978-0-444-51568-1.

Chaumillon, E., Bertin, X., Fortunato, A., Bajo, M., Schneider, J.-L., Dezileau, L., Walsh, J.P., Michelot, A., Chauveau, E., Créach, A., Hénaff, A., Sauzeau, T., Waeles, B., Gervais, B., Jan, G., Baumann, J., Breilh, J.-F., Pedreros, R., 2017. Storm-induced marine flooding: lessons from a multidisciplinary approach. Earth-Sci. Rev. 165, 151–184. https://doi.org/10.1016/j.earscirev.2016.12.005.

Chiu, S., Small, C., 2016. Observations of cyclone-induced storm surge in coastal Bangladesh. J. Coast. Res. 32, 1149–1161. https://doi.org/10.2112/JCOASTRES-D-15-00030.1.

Dokka, R.K., Sella, G.F., Dixon, T.H., 2006. Tectonic control of subsidence and southward displacement of southeast Louisiana with respect to stable North America. Geophys. Res. Lett. 33, L23308. https://doi.org/10.1029/2006GL027250.

Ericson, J.P., Vorosmarty, C.J., Dingman, S.L., Ward, L.G., Meybeck, M., 2006. Effective sea-level rise and deltas: causes of change and human dimension implications. Glob. Planet. Change 50 (1–2), 63–82.

Ferrier, K.L., Mitrovica, J.X., Giosan, L., Clift, P.D., 2015. Sea-level responses to erosion and deposition of sediment in the Indus River basin and the Arabian Sea. Earth Planet. Sci. Lett. 416, 12–20.

Foufoula-Georgiou, E., 2013. A vision for a coordinated effort on delta sustainability. In: Young, G., Perillo, G.M. (Eds.), Deltas: Landforms, Ecosystems and Human Activities, vol. 358. IAHS Publications, Gothenburg, pp. 3–11.

Gebremichael, E., Sultan, M., Becker, R., El Bastawesy, M., Cherif, O., Emil, M., 2018. Assessing land deformation and sea encroachment in the Nile Delta: a radar interferometric and inundation modeling approach. J. Geophys. Res., Solid Earth 123. https://doi.org/10.1002/2017JB015084.

Giosan, L., Syvitski, J., Constantinescu, S., Day, J., 2014. Protect the world's deltas. Nature 516, 31–33. https://doi.org/10.1038/516031a.

Goodbred, S.L., 2003. Response of the Ganges dispersal system to climate change: a source-to-sink view since the last interstade. Sediment. Geol. 162 (1–2), 83–104.

Goodbred, S.L., Kuehl, S.A., 2000a. Enormous Ganges–Brahmaputra sediment discharge during strengthened early Holocene monsoon. Geology 28 (12), 1083–1086.

Goodbred, S.L., Kuehl, S.A., 2000b. The significance of large sediment supply, active tectonism, and eustasy on margin sequence development: Late Quaternary stratigraphy and evolution of the Ganges—Brahmaputra delta. Sediment. Geol. 133 (3–4), 227–248. https://doi.org/10.1016/S0037-0738(00)00041-5.

Goodbred, S.L., Kuehl, S.A., Steckler, M.S., Sarker, M.H., 2003. Controls on facies distribution and stratigraphic preservation in the Ganges–Brahmaputra delta sequence. Sediment. Geol. 155 (3–4), 301–316. https://doi.org/10.1016/S0037-0738(02)00184-7.

Goodbred, S.L., Paolo, P.M., Ullah, M.S., Pate, R.D., Khan, S.R., Kuehl, S.A., Singh, S.K., Rahaman, W., 2014. Piecing together the Ganges–Brahmaputra–Meghna River delta: use of sediment provenance to reconstruct the history and interaction of multiple fluvial systems during Holocene delta evolution. Geol. Soc. Am. Bull. 126 (11–12), 1495–1510.

Grall, C., Henry, P., Tezcan, D., Géli, L., Mercier de Lepinay, B., Rudkiewicz, J.L., Zitter, T., Harmegnies, F., 2012. Heat flow in the Sea of Marmara Central Basin: possible implications for the tectonic evolution of the North Anatolian Fault. Geology. https://doi.org/10.1130/g32192.1.

Hanebuth, T.J.J., Kudrass, H.R., Linstadter, J., Islam, B., Zander, A.M., 2013. Rapid coastal subsidence in the central Ganges–Brahmaputra Delta (Bangladesh) since the 17th century deduced from submerged salt-producing kilns. Geology 41 (9), 987–990.

Higgins, S.A., Overeem, I., Steckler, M.S., Syvitski, J.P.M., Seeber, L., Akhter, S.H., 2014. InSAR measurements of compaction and subsidence in the Ganges–Brahmaputra Delta, Bangladesh. J. Geophys. Res., Earth Surf. 119 (8), 1768–1781.

Hoque, M., Alam, M., 1997. Subsidence in the lower deltaic areas of Bangladesh. Mar. Geod. 20 (1), 105–120.

Hoque, M.A., McArthur, J.M., Sikdar, P.K., Ball, J.D., Molla, T.N., 2014. Tracing recharge to aquifers beneath an Asian megacity with Cl/Br and stable isotopes: the example of Dhakyr, Bangladesh. Hydrogeol. J. 22 (7), 1549–1560.

Horton, B.P., Shennan, I., 2009. Compaction of Holocene strata and the implications for relative sealevel change on the east coast of England. Geology 37 (12), 1083–1086. https://doi.org/10.1130/G30042A.1.

Jankowski, K.L., Törnqvist, T.E., Fernandes, A.M., 2016. Vulnerability of Louisiana's coastal wetlands to present-day rates of relative sea-level rise. Nat. Commun. 8, 14792. https://doi.org/10.1038/ncomms14792.

JICA, 1976. Geology and Stone Material: Jamuna Bridge Construction Project. Tech. rep., Japan International Cooperation Agency, Tokyo.

Karegar, M.A., Dixon, T.H., Malservisi, R., 2015. A three-dimensional surface velocity field for the Mississippi Delta: implications for coastal restoration and flood potential. Geology 43, 519–522. https://doi.org/10.1130/G36598.1.

Karpytchev, M., Ballu, V., Krien, Y., Becker, M., Goodbred, S., Spada, G., et al., 2018. Contributions of a strengthened early Holocene monsoon and sediment loading to present-day subsidence of the Ganges–Brahmaputra Delta. Geophys. Res. Lett. 45, 1433–1442. https://doi.org/10.1002/2017GL076388.

Khan, N.S., Ashe, E., Shaw, T.A., et al., 2015. Holocene relative sea-level changes from near-, intermediate-, and far-field locations. Curr. Clim. Change Rep. 1, 247. https://doi.org/10.1007/s40641-015-0029-z.

Kuehl, S.A., Allison, M.A., Goodbred, S.L., Kudrass, H., 2005. The Ganges–Brahmaputra Delta. In: River Deltas – Concepts, Models, and Examples. In: SEPM Spec. Publ., vol. 83, pp. 413–434.

Lambeck, K., Rouby, H., Purcell, A., Sun, Y.Y., Sambridge, M., 2014. Sea level and global ice volumes from the Last Glacial Maximum to the Holocene. Proc. Natl. Acad. Sci. USA 111 (43), 15296–15303.

Lavier, L., Steckler, M.S., 1998. The effect of sedimentary cover on the flexural strength of continental lithosphere. Nature 392, 843. https://doi.org/10.1038/33974.

Li, C., Czapiga, M.J., Eke, E.C., Viparelli, E., Parker, G., 2015. Variable Shields number model for river bankfull geometry: bankfull shear velocity is viscosity-dependent but grain size-independent. J. Hydraul. Res. 53 (1), 36–48.

Lindsay, J.F., Holliday, D.W., Hulbert, A.G., 1991. Sequence stratigraphy and the evolution of the Ganges–Brahmaputra Delta-complex. Am. Assoc. Pet. Geol. Bull. 75 (7), 1233–1254.

Mallick, B., Rahaman, K.R., Vogt, J., 2011. Coastal livelihood and physical infrastructure in Bangladesh after cyclone Aila. Mitig. Adapt. Strategies Glob. Change 16 (6), 629–648. https://doi.org/10.1007/s11027-011-9285-y.

Marriner, N., Flaux, C., Morhange, C., Kaniewski, D., 2012. Nile Delta's sinking past: quantifiable links with Holocene compaction and climate-driven changes in sediment supply? Geology 40 (12), 1083–1086. https://doi.org/10.1130/G33209.1.

Miall, A.D., Miall, C.E., 2001. Sequence stratigraphy as a scientific enterprise: the evolution and persistence of conflicting paradigms. Earth-Sci. Rev. 54 (4), 321–348. https://doi.org/10.1016/S0012-8252(00)00041-6.

Michels, K.H., Kudrass, H.R., Hubscher, C., Suckow, A., Wiedicke, M., 1998. The submarine delta of the Ganges–Brahmaputra: cyclone-dominated sedimentation patterns. Mar. Geol. 149, 133–154. Earth Planet. Sci. Lett. 386, 75–85. https://doi.org/10.1016/j.epsl.2013.11.003.

Milne, G.A., Mitrovica, J.X., 2008. Searching for eustasy in deglacial sealevel histories. Quat. Sci. Rev. 27, 2292–2302. https://doi.org/10.1016/j.quascirev.2008.08.018.

Montgomery, D.R., Hallet, B., Yuping, L., Finnegan, N., Anders, A., Gillespie, A., Greenberg, H.M., 2004. Evidence for Holocene megafloods down the Tsangpo River gorge, southeastern Tibet. Quat. Res. 62, 201–207. https://doi.org/10.1016/j.yqres.2004.06.008.

Neal, J., Abreu, V., 2009. Sequence stratigraphy hierarchy and the accommodation succession method. Geology 37 (9), 779–782. https://doi.org/10.1130/G25722A.1.

Neidhardt, H., Biswas, A., Freikowski, D., Majumder, S., Chatterjee, D., Berner, Z.A., 2013. Reconstructing the sedimentation history of the Bengal Delta plain by means of geochemical and stable isotopic data. Appl. Geochem. 36, 70–82.

Nienhuis, J.H., Törnqvist, T.E., Esposito, C.R., 2018. Crevasse splays versus avulsions: a recipe for land building with levee breaches. Geophys. Res. Lett. 45, 4058–4067. https://doi.org/10.1029/2018GL077933.

Nittrouer, J.A., Shaw, J., Lamb, M.P., Mohrig, D., 2012. Spatial and temporal trends for water-flow velocity and bed-material sediment transport in the lower Mississippi River. Geol. Soc. Am. Bull. 124 (3–4), 400–414. https://doi.org/10.1130/B30497.1.

O'Grady, D.B., Syvitski, J.P.M., Pratson, L.F., Sarg, J.F., 2000. Categorizing the morphologic variability of siliciclastic passive continental margins. Geology 28, 207–210.

Palamenghi, L., 2012. Tectonic and sea level control on the transport and depositional processes in a siliciclastic sedimentary basin: insights from the Ganges–Brahmaputra Delta, Bengal Basin, Bangladesh.

Paul, B.K., 2009. Why relatively fewer people died? The case of Bangladesh's Cyclone Sidr. Nat. Hazards 50 (2), 289–304. https://doi.org/10.1007/s11069-008-9340-5.

Penland, S., Ramsey, K.E., 1990. Relative sea-level rise in Louisiana and the Gulf of Mexico – 1908–1988. J. Coast. Res. 6 (2), 323–342.

Pickering, J.L., Goodbred, S.L., Reitz, M.D., Hartzog, T.R., Mondal, D.R., Hossain, M.S., 2014. Late Quaternary sedimentary record and Holocene channel avulsions of the Jamuna and Old Brahmaputra River valleys in the upper Bengal Delta plain. Geomorphology 227, 123–136.

Pickering, J.L., Diamond, M.S., Goodbred, S.L., Grall, C., Martin, J.M., Palamenghi, L., Paola, C., Schwenk, T., Sincavage, R.S., Spiess, V., in press. Impact of glacial-lake paleofloods on valley development since glacial termination II: a conundrum of hydrology and scale for the lowstand Brahmaputra–Jamuna paleovalley system. Quat. Sci. Lett.

Reitz, M.D., Pickering, J.L., Goodbred, S.L., Paola, C., Steckler, M.S., Seeber, L., Akhter, S.H., 2015. Effects of tectonic deformation and sea level on river path selection: theory and application to the Ganges–Brahmaputra–Meghna River Delta. J. Geophys. Res., Earth Surf. 120 (4), 671–689.

Revil, A., Grauls, D., Brevart, O., 2002. Mechanical compaction of sand/clay mixtures. J. Geophys. Res., Solid Earth 107 (B11).

Sarker, M.H., Akter, J., Hore, S.K., 2012. Bengal delta not sinking at a very high rate, Daily Star.

Schmidt, C.W., 2015. Delta subsidence: an imminent threat to coastal populations. Environ. Health Perspect. 123 (8). https://doi.org/10.1289/ehp.123-A204.

Schumm, S.A., 1993. River response to base level change – implications for sequence stratigraphy. J. Geol. 101 (2), 279–294.

Shennan, I., 2007. Overview – sea-level studies. In: Scott, A.E. (Ed.), Encyclopedia of Quaternary Science. Elsevier, Amsterdam. ISBN 978-0-444-53642-6, pp. 2967–2974.

Siddique, A.K., Euosof, A., 1987. Cyclone deaths in Bangladesh, May 1985: who was at risk. Trop. Geogr. Med. 39 (1), 57–59.

Sincavage, R., Goodbred, S., Pickering, J., in press. Holocene Brahmaputra River path selection and variable sediment bypass as indicators of fluctuating hydrologic and climate conditions in Sylhet Basin, Bangladesh. Basin Res. https://doi.org/10.1111/bre.12254.

Singh, A., Kirti Bhushan, K., Singh, C., Steckler, M.S., Akhter, S.H., Seeber, L., Kim, W.-Y., Tiwari, A.K., Biswas, R., 2016. Crustal structure and tectonics of Bangladesh: new constraints from inversion of receiver functions. Tectonophysics 680, 99–112. https://doi.org/10.1016/j.tecto.2016.04.046.

Stanley, J.D., Clemente, P.L., 2017. Increased land subsidence and sea-level rise are submerging Egypt's Nile Delta coastal margin. GSA Today 27 (5).

Stanley, D.J., Hait, A.K., 2000. Deltas, radiocarbon dating, and measurements of sediment storage and subsidence. Geology 28 (4), 295–298.

Steckler, M.S., ten Brink, U.S., 1986. Lithospheric strength variations as a control on new plate boundaries: examples from the Arabian Plate. Earth Planet. Sci. Lett. 79, 120–132.

Steckler, M.S., Akhter, S.H., Seeber, L., 2008. Collision of the Ganges–Brahmaputra Delta with the Burma Arc: implications for earthquake hazard. Earth Planet. Sci. Lett. 273 (3–4), 367–378.

Steckler, M.S., Mondal, D.R., Akhter, S.H., Seeber, L., Feng, L.J., Gale, J., Hill, E.M., Howe, M., 2016. Locked and loading megathrust linked to active subduction beneath the Indo-Burman Ranges. Nat. Geosci. 9 (8), 615.

Stein, C.A., Stein, S., 1992. A model for the global variation in oceanic depth and heat-flow with lithospheric age. Nature 359 (6391), 123–129. https://doi.org/10.1038/359123a0.

Stuiver, M., Reimer, P.J., 1993. Extended C-14 data-base and revised Calib 3.0 C-14 age calibration program. Radiocarbon 35 (1), 215–230.

Syvitski, J.P.M., et al., 2009. Sinking deltas due to human activities. Nat. Geosci. 2 (10), 681–686.

Talwani, M., Desa, M.A., Ismaiel, M., Sree Krishna, K., 2016. The tectonic origin of the Bay of Bengal and Bangladesh. J. Geophys. Res., Solid Earth 121, 4836–4851. https://doi.org/10.1002/2015JB012734.

Tessler, Z.D., Vorosmarty, C.J., Grossberg, M., Gladkova, I., Aizenman, H., Syvitski, J.P.M., Foufoula-Georgiou, E., 2015. Profiling risk and sustainability in coastal deltas of the world. Science 349 (6248), 638–643.

Tornqvist, T.E., Wallace, D.J., Storms, J.E.A., Wallinga, J., Van Dam, R.L., Blaauw, M., Derksen, M.S., Klerks, C.J.W., Meijneken, C., Snijders, E.M.A., 2008. Mississippi Delta subsidence primarily caused by compaction of Holocene strata. Nat. Geosci. 1 (3), 173–176.

Trampush, S.M., Huzurbazar, S., McElroy, B., 2014. Empirical assessment of theory for bankfull characteristics of alluvial channels. Water Resour. Res. 50 (12), 9211–9220.

Umitsu, M., 1993. Late Quaternary sedimentary environments and landforms in the Ganges Delta. Sediment. Geol. 83 (3–4), 177–186.

Vernant, P., Bilham, R., Szeliga, W., Drupka, D., Kalita, S., Bhattacharyya, A.K., Gaur, V.K., Pelgay, P., Cattin, R., Berthet, T., 2014. Clockwise rotation of the Brahmaputra Valley relative to India: tectonic convergence in the eastern Himalaya, Naga Hills, and Shillong Plateau. J. Geophys. Res., Solid Earth 119 (8), 6558–6571. https://doi.org/10.1002/2014JB011196.

Waelbroeck, C., Labeyrie, L., Michel, E., Duplessy, J.C., McManus, J.F., Lambeck, K., Balbon, E., Labracherie, M., 2002. Sea-level and deep water temperature changes derived from benthic foraminifera isotopic records. Quat. Sci. Rev. 21 (1–3), 295–305.

Walker, M.J.C., Berkelhammer, M., Björck, S., Cwynar, L.C., Fisher, D.A., Long, A.J., Lowe, J.J., Newnham, R.M., Rasmussen, S.O., Weiss, H., 2012. Formal subdivision of the Holocene series/epoch: a discussion paper by a Working Group of INTIMATE (Integration of ice-core, marine and terrestrial records) and the Subcommission on Quaternary Stratigraphy (International Commission on Stratigraphy). J. Quat. Sci. 27, 649–659. https://doi.org/10.1002/jqs.2565.

Waschbusch, P.J., Royden, L., 1992. Episodicity in foredeep basins. Geology 20, 915–918.

Wheeler, H.E., 1964. Base level, lithosphere surface, and time-stratigraphy. Geol. Soc. Am. Bull. 75 (7), 599–609.

Wilson, C.A., Goodbred, S.L., 2015. Construction and maintenance of the Ganges–Brahmaputra Meghna Delta: linking process, morphology, and stratigraphy. Annu. Rev. Mar. Sci. 7, 67–88. https://doi.org/10.1146/annurev-marine-010213-135032.

Zahid, K.M., Uddin, A., 2005. Influence of overpressure on formation velocity evaluation of Neogene strata from the eastern Bengal Basin, Bangladesh. J. Asian Earth Sci. 25, 419–429. https://doi.org/10.1016/j.jseaes.2004.04.003.